Research article

Zhenfei Li, Malin Premaratne and Weiren Zhu*

Advanced encryption method realized by secret shared phase encoding scheme using a multi-wavelength metasurface

https://doi.org/10.1515/nanoph-2020-0298
Received May 21, 2020; accepted June 19, 2020; published online July 4, 2020

Abstract: Multi-channel information encryption technology has been implemented by optical metasurfaces owing to their superior ability to control the phase, amplitude, wavelength and polarization of incident light. However, current metasurface-based multi-channel encryption technologies suffer from information leakage in non-full channel decoding processes. To better increase the security of the encrypted information, we develop a secret shared phase encoding scheme by combining a visual secret sharing scheme with a metasurface-based phase-encoding technique. Our method achieves its high-concealment through mapping the target image into a set of unrecognizable phase-only keys that are subsequently encoded by a multi-wavelength metasurface. In the decryption process, the secret information can be reconstructed only by decoding and stacking all the wavelength channels of the metasurface. At the same time, chaotic images can be extracted from the other channels without revealing any original information. The simulated results and the theoretical analysis show the strong robustness and high security of our encryption setup, which is sure to find applications in emerging optical encryption schemes.

Keywords: information encryption; metasurface; multi-wavelength; phase encoding; secret sharing.

***Corresponding author: Weiren Zhu**, Department of Electronic Engineering, Shanghai Jiao Tong University, Shanghai, 200240, China, E-mail: weiren.zhu@sjtu.edu.cn. https://orcid.org/0000-0002-6568-738X
Zhenfei Li: Department of Electronic Engineering, Shanghai Jiao Tong University, Shanghai, 200240, China, E-mail: zhenfei-li@sjtu.edu.cn
Malin Premaratne: Advanced Computing and Simulation Laboratory (AχL), Department of Electrical and Computer Systems Engineering, Monash University, Clayton, 3800, Victoria, Australia, E-mail: malin.premaratne@monash.edu

1 Introduction

With the increasing importance of information security, numerous cryptographic techniques using optical means by manipulating the features of the optical wave-front of an information-carrying beam have been proposed and developed [1]. In particular, optical metasurfaces [2–6], the ultrathin synthesized engineering interfaces consisting of sub-wavelength unit cells, are emerging as promising candidates for information security applications owing to their offered superior capability in manipulating phase, amplitude, wavelength and polarization as information security keys. Recently, it has been reported that information encryption could be realized by optical metasurface holography [7–10], which provides an effective way to imprint the secret information by transforming the visible target images into the unrecognizable phase-only distributions based on phase-encoding technology [11–14]. The corresponding secret images can be directly extracted by optical diffraction only if one knows the predesigned wavelength or polarization. In the metasurface-based phase encoding technology, secret images are encoded to be directly invisible but recoverable via phase-dependent decoding keys.

The enhanced flexibility in wave-front manipulation over different physical dimensions in a metasurface makes it possible to encode multiple independent information channels with high security. There are several reported cases of the use of multi-channel metasurfaces for encoding in literature. For example, in the multi-wavelength encoding process [15–18], an image was first decomposed into multi-images and encoded to a single metasurface composed of resonant multiplexing units, which behaves differently based on the wavelength of light interacting with it. Therefore, it is possible to decode information on various decomposed multi-images using distinct probing wavelengths on the metasurace. In another scheme, the decomposed image is encoded using the metasurface's polarization-selectivity, either by using a pair of orthogonal linear polarization states [19, 20] or by using the

helicity polarization channels [21, 22]. Also, there are schemes where both the above features have been combined and used simultaneously [23–25]. Recent reports also show that features such as diffraction position [26], incident angles [27], nonlinearity [28], and orbital angular momentum (OAM) [29] have been successfully exploited in optical encryption schemes.

Information encryption based on multi-channel metasurface encoding approaches can dramatically improve information security owing to combining multiple possible degrees of freedom. However, in the single-channel decoding processes in such metasurfaces, the extracted results are directly-exposed and mutually-coupled with other channels. This is security vulnerability, because it possible uses this information leak due to coupling to extract the original information. Contrary to this, in this paper, we first propose a novel secret shared phase encoding (SSPE) scheme for high-level information encryption by combing visual secret sharing (VSS) scheme [30, 31] with multi-wavelength metasurface holography. Therein, VSS scheme provides a basic encryption scheme that can encode information into n seemingly-random and mutually-unrelated shared keys (SKs) [30, 31], ensuring that the information is fully concealed for less than n shares, while the multi-wavelength holography gives the enhanced security for the secret information. Our method has obvious advantages and higher security compared to traditional metasurface-based spatial multiplexing encryption technologies which suffer from information leakage in any non-full channel decoding processes. For fully illustrating the feasibility and universality, the cases of multiple metasurfaces, spatial multiplexing and non-interleaved multi-wavelength metasurface are all discussed in this paper. The simulation results and theoretical analysis reveal the high-security, that is, the secret information can be recovered only by decoding and stacking all the possible channels of the metasurface while meaningless images get extracted otherwise. The proposed method provides a more secure and simple strategy for implementing information encryption and may incite interest in research community the value and feasibility of experimental demonstration of the laid out concept in the future.

2 Principle and design

The innovation of this work is to propose an advanced encryption method, rather than to design a new type of metasurfaces, and thus, a general spatial multiplexing multi-wavelength metasurface is used to verify this strategy. Figure 1 illustrates the schematic diagram of SSPE scheme using multi-wavelength metasurface, which consists of three types of nanoblocks with spatially varying rotation angles multiplexed in a subwavelength unit, enabling to resonate with three different wavelengths of red, green and blue. In the encoding process, the secret image "SJTU" is decomposed into three set of SKs based on the encryption algorithm of (3, 3) VSS scheme. Three visible wavelengths of red, green and blue are chosen as three independent channels to encode the target images of the three SKs, respectively. These SKs are transformed into the corresponding phase-only keys (POKs) by multi-wavelength phase encoding and then encoded into the metasurface. The decoding can be carried out by illuminating the metasurface with either of the red, green, or blue light, exploiting its resonant characteristics. Based on the SSPE scheme, we can recover the original information "SJTU" by using the correct three-color illumination sequence. Any other illumination sequence would only generate a nonsensical image (or chaotic image) with no valuable information.

2.1 SSPE scheme with multiple metasurfaces

Before introducing the SSPE scheme based on multi-wavelength metasurface, we first consider a simple case that all SKs are wavelength-independent and encoded into multiple metasurfaces. The corresponding encryption process is shown in Figure 2(a), which relies on the following three steps: 1) VSS encoding, 2) single wavelength phase encoding and 3) metasurface recoding.

Step 1: As a well-recognized and highly-security encryption approach, the idea of VSS is employed as one of the

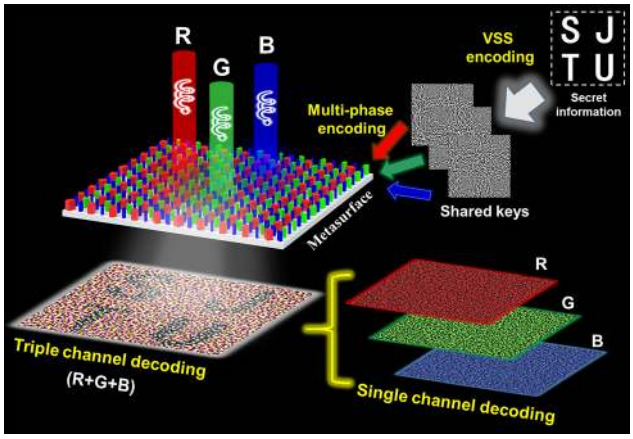

Figure 1: Schematic diagram of the SSPE scheme with multi-wavelength metasurface.

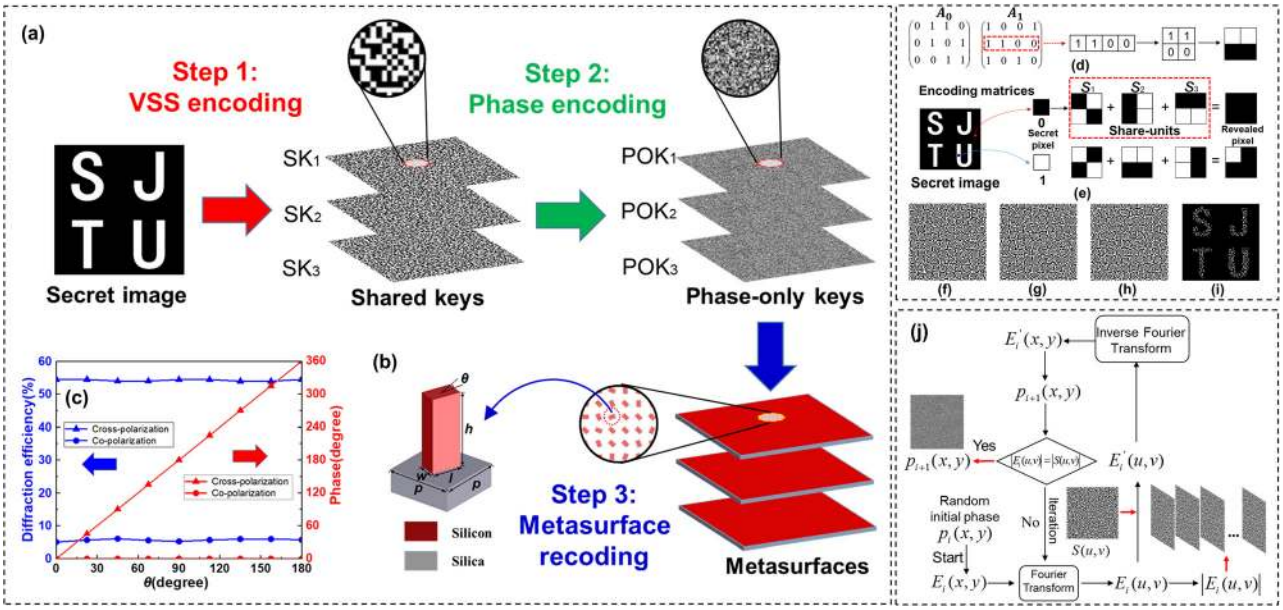

Figure 2: Encryption principle of the proposed SSPE scheme with multiple metasurfaces. (a) Schematic for the corresponding encryption process. (b) Structure unit of metasurface. (c) Simulated diffraction efficiency and phase of the cross-polarized and co-polarized parts. (d–i) The principle of (3, 3) VSS scheme. (j) The flowchart of GS phase retrieval algorithm.

key technology in the proposed SSPE scheme. Therein, the (3, 3) VSS describes a 3-out-3 secret sharing scheme that enables to convert the secret image to 3 mutually-unrelated SKs and distribute them to three participants so that any t (t < 3) of n combinations of authorized participants can reconstruct the target information. Consider a binary image with spatial coordinates (i = 1,2, … ,m and j = 1,2, … ,n), mapped to a matrix with element values of 0 and 1, where a white pixel is represented as p_{ij} = 1, while a black pixel is denoted as p_{ij} = 0. In the (3, 3) VSS encoding process, each pixel of the secret image is decomposed into four sub-pixels (2 × 2 array) composed of black and white blocks in each of three share-units (s_1, s_2, s_3) via the encoding function $f(p_{i,j})$, which is given by:

$$f(p_{i,j}) = \begin{cases} [s_1, s_2, s_3]^{\mathrm{T}} \in C_0 & p_{i,j} = 0, \\ [s_1, s_2, s_3]^{\mathrm{T}} \in C_1 & p_{i,j} = 1, \end{cases} \quad (1)$$

where C_0 and C_1 are the matrix collections, obtained by performing a column transformation of the two basis encoding matrices (A_0, A_1), as shown in Figure 2(d). If the pixel of the secret image is black, $p_{i,j}$ = 0 (white, i.e., $p_{i,j}$ = 1), one combination of $[s_1, s_2, s_3]^T$ is randomly selected from the set of C_0 (C_1) as the ciphertext of blocks in SK_1, SK_2 and SK_3, respectively. The generating process of the share-unit for (1100), i.e., the second row of A_1, is shown in Figure 2(d). Each block of the sub-pixels has A_4^4 (full permutation of columns) sets of alternative share-units for both black and white secret pixels. Figure 2(e) gives an example of such encoding process for each secret black and white pixel. Obviously, a single share-unit of s_1, s_2 or s_3 cannot reveal any clue of the secret black and white pixels. As these three share-units stacking together, four black sub-pixel blocks appear if the secret pixel is black, while one white sub-pixel block and three black sub-pixel blocks appear if the secret pixel is white. According to the (3, 3) VSS scheme, the target image "SJTU" (50 × 50 pixel array) can be encoded into the three SKs (each for 100 × 100 sub-pixel array), as shown in Figure 2(f–h), which look like a random checker-board array without leakage of original information. By stacking all three SKs, the secret information can be recovered, with the corresponding decoding result is shown in Figure 2(i).

Step 2: Phase encoding. VSS encoding ensures message security by encoding the secret information into meaningless, mutually unrelated SKs and then the security can be further extended by hiding the SKs into the POKs with high imperceptibility and strong robustness. Here, the classic Fourier domain Gerchberg–Saxton (GS) phase retrieval algorithm [13, 14] is employed for transforming the three SKs into unrecognized three POKs. The flowchart of the GS algorithm is presented in Figure 2(j), which utilizes an iterative process between the image plane and the hologram plane via the Fourier transform and inverse Fourier transform. The whole iterative process starts at the

hologram plane with an initial random phase. After performing multiple iterations, the desired POK can be extracted correctly by observing whether it can project the corresponding target image of SK. Considering that the reconstructed images of SKs are composed of discrete spots-like images rather than continuum images, we should discretize as many pixel values as possible during the phase encoding process in order to make the reconstructed image have a higher resolution and perfectly reproduce the original information. Through reasonable parametric optimization, we found that when the sub-pixel corresponds to 5×5 or more meta-atoms, the edge characteristics of the white or black sub-pixels of SKs can be well reproduced. When the meta-atoms are fewer, the reconstructed sub-pixels will be distorted. Therefore, in order to ensure a high quality of holographic image from the metasurface, each black or white sub-pixel of SKs is composed of 5×5 sub-phase array and the corresponding POKs are discretized in eight-level from 0 to 360° with the increment of 45°.

Step 3: Metasurface recoding. As mentioned before, the encoding process in steps 1 and 2 can transform the secret information into a set of POKs with high imperceptibility. To encode the calculated POKs onto the metasurface, silicon nanoblocks with relatively mature processing technology in the visible range are employed as basic mask elements to imprint the calculated phase information. Although the absorption loss of Si gradually increases with the blue shift of the wavelength, which can be overcome by using the optical transparency materials [32, 33] (e.g., SiN or TiO_2), higher aspect ratio seriously increases the fabrication complexity and hence may cause additional scattering losses and phase errors. As shown in Figure 2(b), each silicon nanoblock is designed with length $l = 140$ nm, width $w = 100$ nm, height $h = 320$ nm and the entire silicon nanoblocks are arranged on the top of a silica substrate with the unit period of 350 nm. Pancharatnam–Berry phase [34, 35] is adopted to realize phase modulation and each kind of the designed nanoblocks with sub-wavelength sizes can be served as half-wave plate for the operation wavelength of 632.8 nm, which can cover phase profiles from 0 to 360° with in-plane orientation changing from 0 to 180°. Figure 2(c) shows the simulated diffraction efficiency and phase distributions of the cross-polarized and co-polarized transmission components with the rotation angle of the nanoblock vary from 0 to 180° for left-handed circularly polarized light.

After the above-mentioned three steps, the secret image "SJTU" is transformed into three unrecognized and meaningless phase-only metasurface holograms. The finite difference time domain (FDTD) method is employed to decrypt the hidden information in SSPE. By illuminating the corresponding metasurface holograms with appropriate wavelength channels, the reconstructed holographic images of SKs are obtained by:

$$E_i(u, v) = \left|\mathrm{FT}\{p_i(x, y)\}\right|^2, \tag{2}$$

where FT is Fourier transform, capable of converting the unrecognizable POKs into the visual pure-amplitude SKs patterns, $1 \le i \le 3$ represents different metasurface holograms, $p_i(x,y)$ is the POK in the ith hologram. In order to decrypt the secret image "SJTU", we need to stack and align all the extracted SKs based on the SSPE scheme, which is given by:

$$E(u, v) = \sum_{i}^{3} E_i(u, v). \tag{3}$$

According to Eqs. (2) and (3), simulation results of normalized intensity patterns are extracted and shown in Figure 3 with original SKs and stacking result as references. Figure 3(e–g) shows the reconstructed images of SKs decoded by corresponding wavelength at 632.8 nm. The enlarged regions within the solid circle in the simulated SKs are there for comparison with the original results in Figure 3(a–c). Obviously, the extracted SKs coincide with the original SKs except the presence of low levels of random noise due to phase discretization errors, verifying the accuracy of the decoding results. By stacking and aligning all the extracted SKs, the original secret information "SJTU" can be recovered, as shown in Figure 3(h), which is also consistent with the original information in Figure 3(d). It should be noted that the superimposing mechanisms of the traditional VSS and SSPE schemes are different. In the VSS scheme, the stacking process relies on the transmission of light, so that light through the SKs printed on transparencies will be blocked by black pixels, which follows the logical "AND" defined mathematically as: $1 \cap 1 = 1$, $0 \cap 1 = 0$, $1 \cap 0 = 0$, $0 \cap 0 = 0$. However, the superposition of SKs in SSPE depends on the reflection of light so that original black blocks can be illuminated by the bright blocks of other channels, which follows the logical "OR" defined mathematically as: $1 \cup 1 = 1$, $0 \cup 1 = 1$, $1 \cup 0 = 1$, $0 \cup 0 = 0$. Therefore, in contrast to the traditional VSS scheme; where the staked shares of white secret pixel is only 1/4 white, directly resulting in a loss of 3/4 original information as shown in Figure 3(d). The SSPE scheme in our design can preserve original information because the original black pixel blocks are illuminated by bright

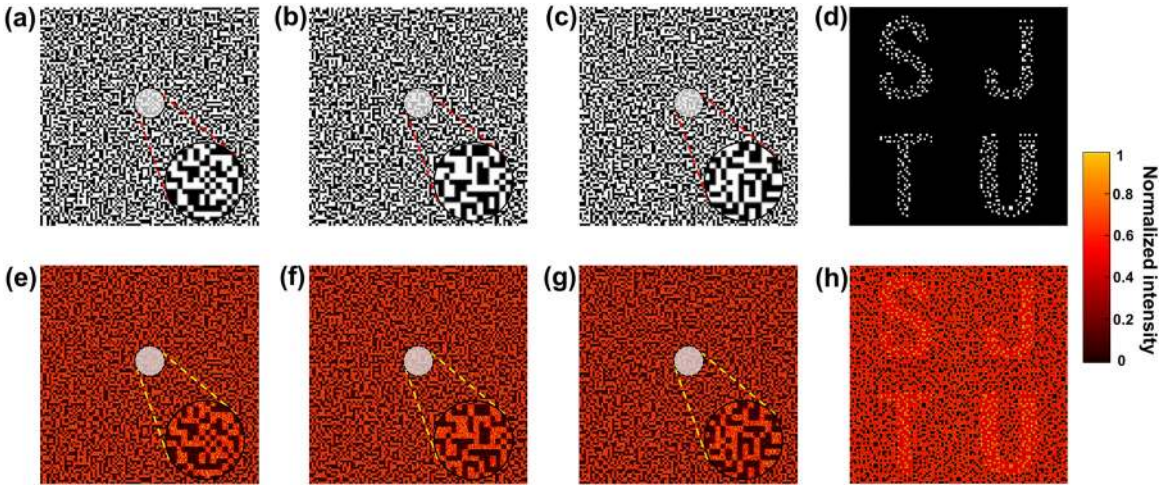

Figure 3: Original reference results and simulation results of the SSPE scheme with multiple metasurfaces. (a–c) Original SKs and (d) stacking result. (e–g) Reconstructed images of SKs and (h) corresponding revealed result.

colors, resulting in the presentation of lost black subpixel blocks as shown in Figure 3(h).

2.2 SSPE scheme with a multi-wavelength metasurface

Based on the resonance characteristics of nano-structured elements [36], the SSPE scheme can be further extended to realize multi-wavelength phase encoding by multiplexing multiple resonance units in a supercell, which can resonantly interact with the corresponding operation wavelengths. Here, we chose three primary wavelengths of red (632.8 nm), green (532 nm) and blue (473 nm) as the three independent wavelength channels to encode the visual SKs into three POKs, i.e., POK_R at 632.8 nm, POK_G at 532 nm, and POK_B at 473 nm. Pancharatnam–Berry phase principle is also adopted to realize phase modulation because of its wavelength independent characteristic. It is worth noting that the Pancharatnam–Berry phase typically has a broadband phase response. Although a certain amount of wavelength shift may not cause much influence on the reconstruction information, the transmission efficiency strongly relies on the resonance characteristics of nano-structured elements, which can be tuned by their shapes and dimensions. Careful choices of the geometric sizes, the response wavelengths of the nanoblocks can be limited around red, green and blue wavelengths. In this design, three silicon nanoblocks with different dimensions are employed and integrated into a supercell, each can response to one of the three typical wavelengths individually. The supercell with a period of 400 nm of the multi-wavelength metasurface used in our design is shown in Figure 4(a). It is composed of three kinds of colored silicon nanoblocks marked by the S_R, S_G and S_B, where the red one is capable of responding to the incident beam at 632.8 nm, the green one at 532 nm, and the blue two are at 473 nm to compensate for high absorption losses [18]. The corresponding dimensions of the S_R, S_G and S_B are shown in Figure 4(b). Figure 4(c) shows the simulated diffraction efficiency of an individual nanoblock of S_R, S_G and S_B for incident of left-handed circularly polarized (LHCP) light spanning the wavelength range from 450 to 750 nm. The resonance peaks correspond to three designed colors (R, G and B), which proves the correctness of the design and the insignificant cross-talks between different wavelength channels. Figure 4(d–f) shows the top views of the simulated optical energy distributions with the different wavelength of R, G and B. It is clearly that energy is strongly confined in the nanoblocks with negligible interactions in each pixel units, so that the corresponding phase masks for each wavelength can be independently manipulated.

The flowchart of the corresponding SSPE algorithm with multiple wavelengths metasurface is shown in Figure 5. The target image "SJTU" is firstly encoded into three SKs using (3, 3) VSS encryption scheme. Then the three SKs of SK_1, SK_2 and SK_3 are re-colored with three color components of λ_R, λ_G and λ_B, respectively. Since the secret image is revealed by staking all the three reconstructed SKs, the three share components of the color holographic image in the RGB channels should be adjusted to make the size match at the same imaging position. For an M × M hologram, the pixel size of the diffracted pattern in far-field can be calculated by $\Delta p = \lambda_i d/M\Delta f_p$, where λ_i represents different wavelength components, d is diffraction distance, Δf_p is pixel size of the hologram [10]. Obviously, the larger

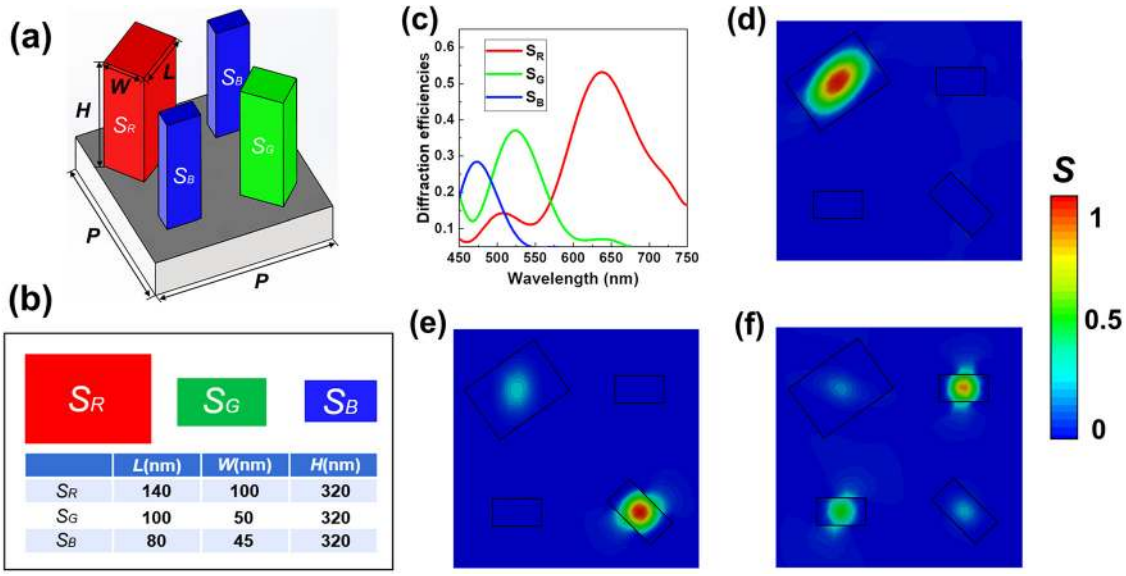

Figure 4: Illustration of the supercell. (a) One supercell composed of three kind of Si nanoblocks (b) Three Si nanoblocks with different dimension. (c) Simulated transmission spectra of an individual nanoblock of S_R, S_G and S_B. (d–f) Top views of the optical energy distributions with the different wavelengths of R, G and B.

wavelength is required for smaller number of pixels in the object plane. In order to make the size of the holographic image independent of the wavelength, the number of pixels and the corresponding wavelengths in RGB channels should follow $m_R:m_G:m_B = 1/\lambda_R: 1/\lambda_G: 1/\lambda_B$. So, in this design, we set the number of pixels for each share component as 374×374 in SK_R, 420×420 in SK_G, 500×500 pixels in SK_B, respectively. The effective area of the reconstructed image is determined by the number of samples in the blue channel. Thus, to integrate all the components into one hologram, the redundant edge areas of the SK_R and the SK_G are padded with zeros, so that the three-components of POK_R, POK_G and POK_B have the same number of 500×500 pixels.

As the decoding of SSPE scheme is wavelength dependent, in the SSPE scheme, the shared blocks with different colors could be extracted by the corresponding visible wavelength of R, G and B. To elucidate the multi-wavelength decoding scheme, we employ (RGB) to describe a shared color block, with the black block of

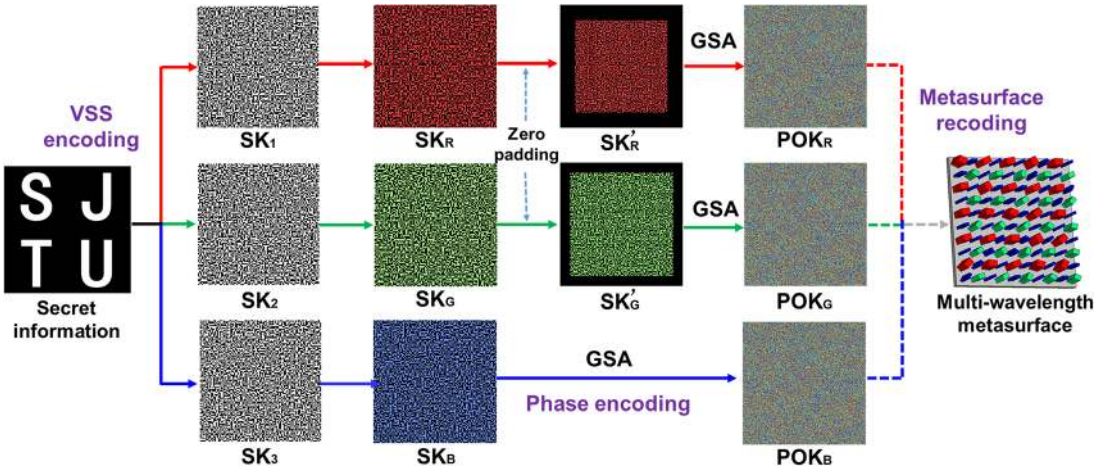

Figure 5: A flowchart of SSPE algorithm to generate a set of shared phase-only keys.

(000), red block of (100), green block of (010) and blue block of (001), the corresponding decoding collections of D_0 and D_1 are obtained by permuting the columns of the following two basic multi-color decoding matrices:

$$D_0 = \begin{bmatrix} 000, 100, 100, 000 \\ 000, 010, 000, 010 \\ 000, 000, 001, 001 \end{bmatrix}, \quad D_1 = \begin{bmatrix} 100, 000, 000, 100 \\ 010, 010, 000, 000 \\ 001, 000, 001, 000 \end{bmatrix}.$$

So, the stacked blocks should be composed of the following eight kinds of color combinations: (000) for black, (100) for red, (010) for green, (001) for blue, (110) for yellow, (011) for cyan, (101) for magenta and (111) for white. Figure 6 shows the graphical interpretation of six (out of 24) possible combinations of the extracted results by stacking the three shared color blocks of S_R, S_G and S_B. If the secret pixel is white, the stacked result of S_R, S_G and S_B will be presented in a random combination of red, green, blue (R, G, B) and white blocks, while the arbitrary combination of cyan, yellow, magenta (C, Y, M) and black blocks will be displayed for the secret black pixel.

Figure 7 shows the simulated holographic images in the case of single, dual and triple channels rendered by the multi-color decoding matrix mentioned above. Under the incident of three fundamental channel states of R, G and B, the extracted monochromatic images of SKs are shown in Figure 7(a–c). As expected, the extracted SKs have the identical sizes for the three wavelengths, making it possible for us to recover the compound channels by manipulating the combinations of the three fundamental states. By comparing the partial enlarged region of the simulated SKs with the original SKs in Figure 3(a–c), it is clear that the extracted results are closely matches with the original SKs despite some negligible shadows of other SKs both in G-channel and B-channel. Simulation results also indicate that the diffracted efficiencies of the reconstructed SKs are 34% at R, 12.3% at G, and 7.8% at B, respectively, which are evidently lower than those of single Si nanoblocks because of the rising reflection and absorption losses with the number of multi-color nanoblocks in each supercell [18]. In order to improve the diffraction efficiency, we also designed another non-interlaced metasurface and provide a comparison with spatial multiplexing method in Section 1 of the Supplementary material. By arbitrarily selecting two out of three fundamental states (R + G, G + B and R + B), the colorful block patterns combining the primary colors (R, G and B) with their secondary colors (Y, C and M) can be created as shown in Figure 7(d–f). Obviously, only the mosaic-like patterns with different colors are extracted both in single channel and dual channel decoding processes, that reveal none of the original secret information. Only in the triple channel decoding process, the recovered secret image "SJTU" can be reconstructed, as shown in Figure 7(g), which is displayed in full set of colors (including white and black colors). Although the contrast of the revealed secret image is unsatisfactory, as a result of the "SJTU" is drowned in the dazzling background color, the quality of the decoded result is acceptable for the naked eye. Furthermore, in Section 2 of the Supplementary material, we also consider and discuss another reciprocal VSS encoding scheme. That is, the black pixel of secret image is randomly selected from C_1 while the white pixel is randomly selected from C_0.

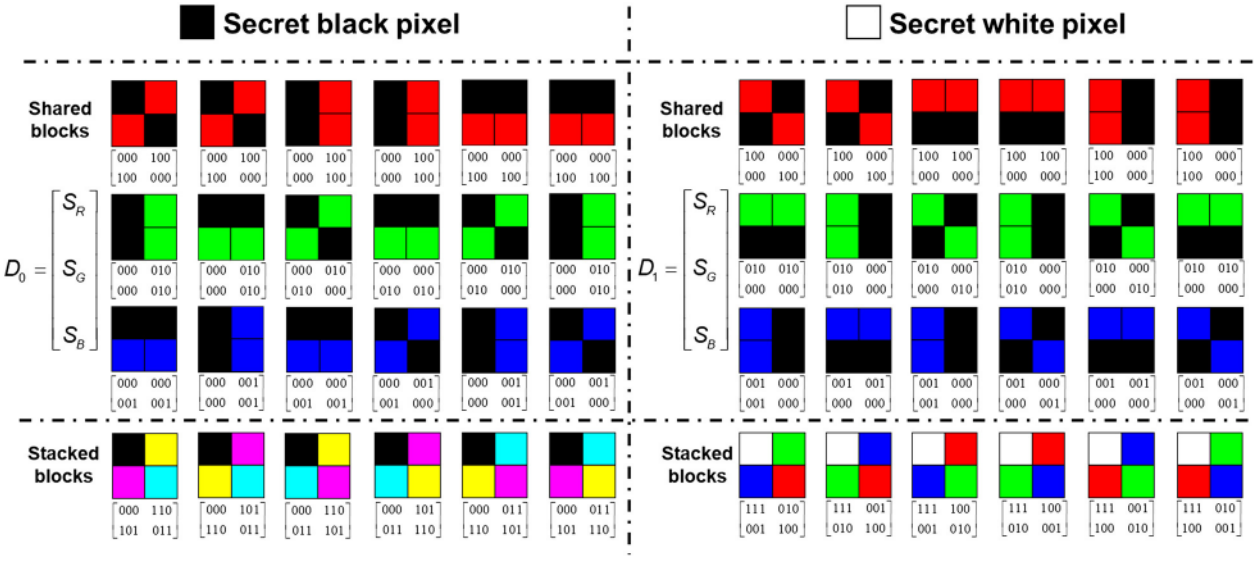

Figure 6: Graphical interpretation of six of 24 possible combinations of decoding matrices.

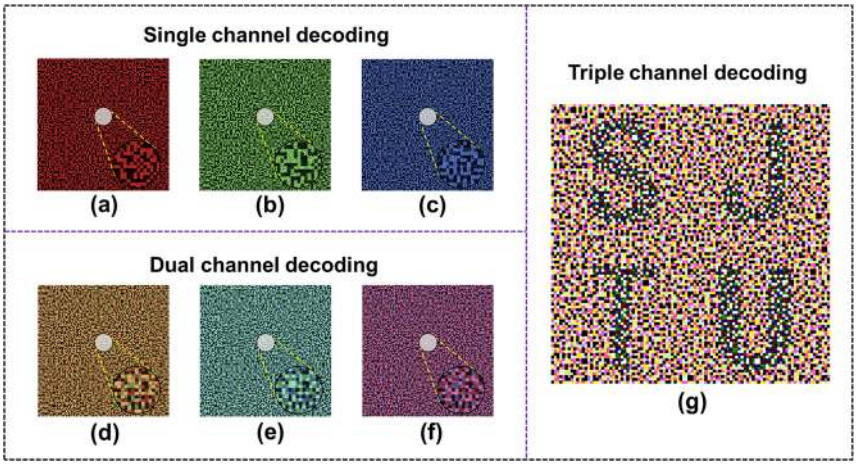

Figure 7: Simulated intensity patterns rendered by the multi-color decoding matrix. Extracted images of SKs decoded by (a–c) single channel, (d–f) dual channels, and (g) triple channels.

3 Analysis and discussion

Robustness and security are two important attributes for any good encryption algorithm. The proposed SSPE scheme integrates the VSS with metasurface holography, making it a highly robust and secure algorithm. To establish the accuracy and validity of the proposed encryption scheme, we carry out several theoretical investigations here.

First, we consider the robustness attribute of the SSPE scheme. Consider the case where the phase distortion results eminating from errors in the manufacturing process due to handling. We can emulate this by adding phase noises directly to the phase masks to evaluate the quality of the extracted image. The recovered secret image can be written as by:

$$E'(u, v) = \sum_{i=1}^{3} \left| \mathrm{FT}\left\{ p_i(x, y) e^{a\varphi_i^{\mathrm{rand}}} \right\} \right|^2, \tag{4}$$

where $p_i(x,y)$ is the original phase distribution in the ith hologram, $\varphi_i^{\mathrm{rand}}$ is the random phase noise in the same hologram with the range from 0 to 2π, a is the noise correlation factor with the range from 0 to 1. The correlation coefficient (Co) is employed to evaluate the robustness of the encryption system. The value of Co is defined as:

$$Co(E, E') = Cov(E, E')(\sigma_E \sigma_{E'})^{-1}, \tag{5}$$

where E and E' are the decoded secret images with and without the phase noise, respectively, $Cov(E, E')$ is the cross-covariance between E and E', σ is standard deviation. The value of Co in the range of [0, 1] represents the similarity of the two revealed results, with the maximum represents the best quality and the minimum means the worst quality of corresponding decoding results. With noise correlation increasing from 0 to 1, the value of Co drops down slowly and keeps a relatively high level over a wide range of noise values, as shown in Figure 8. We note that the quality of the recovered results gradually deteriorates until it cannot be recognized. The recovered results show that the SSPE scheme still has a 65% noise tolerance, which is a good indicator for the robust anti-noise capability of the encryption system.

Next, we perform an analysis of the strength of the security provided by the algorithm. The multi-wavelength metasurface used in proposed encryption system possesses three independent wavelength channels, which are used as security keys to decrypt the SKs. In other words, it is possible to decrypt the target image only illuminating the metasurface in the pre-designed wavelength components or their combinations. On the other hand, the SSPE scheme inherits the high security of VSS, so that only meaningless information would be extracted in the case of non-full-channel decoding process, without any leakage of secret information. In Section 3 of the Supplementary material, we further evaluate the security

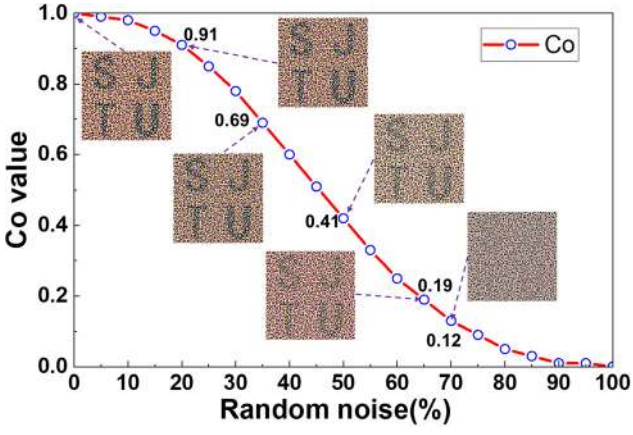

Figure 8: Noise analysis of SSPE scheme.

level of SSPE scheme based on the principle of VSS. All these properties of SSPE scheme with multi-wavelength metasurface are beneficial to maintaining the high security of secret information.

4 Conclusion

In summary, we have proposed and demonstrated theoretically an SSPE scheme by combining VSS scheme with multi-wavelength metasurface phase encoding technology. In the encoding process, the target information is decomposed into three sets of SKs, which are transformed into the corresponding POKs by phase encoding algorithm and then encoded into the three-wavelength metasurface. In the decryption process, each calculated phase-dependent key can project the corresponding intensity pattern of the SKs under the illumination of red, green or blue light, individually. The secret information can be recovered only when the light of the three designed wavelengths are simultaneously illuminated onto the metasurface, while meaningless patterns would be extracted in other cases. Besides, strong anti-noise and high security have been demonstrated, making such an encryption system suitable for future development of optical image encryption, hiding, anti-counterfeiting, or information authentication.

Acknowledgments: This work was supported by National Natural Science Foundation of China (NSFC) (61701303, 51777168), Natural Science Foundation of Shanghai (17ZR1414300).

Author contribution: All the authors have accepted responsibility for the entire content of this submitted manuscript and approved submission.

Research funding: This work was supported by National Natural Science Foundation of China (NSFC) (61701303, 51777168), Natural Science Foundation of Shanghai (17ZR1414300).

Conflict of interest statement: The authors declare no conflicts of interest regarding this article.

Reference

[1] W. Chen, B. Javidi, and X. Chen, "Advances in optical security systems," *Adv. Optic Photon*, vol. 6, pp. 120–155, 2014.

[2] N. Yu, P. Genevet, M. A. Kats, et al., "Light propagation with phase discontinuities: generalized laws of reflection and refraction," *Science*, vol. 334, pp. 333–337, 2011.

[3] S. M. Kamali, E. Arbabi, A. Arbabi, and A. Faraon, "A review of dielectric optical metasurfaces for wavefront control," *Nanophotonics*, 2018, vol. 7, no. 6, pp. 1041–1068.

[4] A. V. Kildishev, A. Boltasseva, and V. M. Shalaev, "Planar photonics with metasurfaces," *Science*, vol. 339, p. 1232009, 2013.

[5] N. I. Zheludev and Y. S. Kivshar, "From metamaterials to metadevices," *Nat. Mater.*, vol. 11, pp. 917–924, 2012.

[6] A. E. Minovich, A. E. Miroshnichenko, A. Y. Bykov, T. V. Murzina, D. N. Neshev, and Y. S. Kivshar, "Functional and nonlinear optical metasurfaces," *Laser Photon. Rev.*, vol. 9, pp. 195–213, 2015.

[7] P. Genevet and F. Capasso, "Holographic optical metasurfaces: a review of current progress," *Rep. Prog. Phy.*, vol. 78, p. 024401, 2015.

[8] W. Wan, J. Gao, and X. Yang, "Metasurface holograms for holographic imaging," *Adv. Opt. Mater.*, vol. 5, p. 1700541, 2017.

[9] X. Ni, A. V. Kildishev, and V. M. Shalaev, "Metasurface holograms for visible light," *Nat. Commun.*, vol. 4, p. 2807, 2013.

[10] G. Zheng, H. Mühlenbernd, M. Kenney, G. Li, T. Zentgraf, and S. Zhang, "Metasurface holograms reaching 80% efficiency," *Nat. Nanotechnol.*, vol. 10, pp. 308–312, 2015.

[11] P. Refregier and B. Javidi, "Optical image encryption based on input plane and Fourier plane random encoding," *Opt. Lett.*, vol. 20, pp. 767–769, 1995.

[12] B. Javidi and T. Nomura, "Securing information by use of digital holography," *Opt. Lett.*, vol. 25, pp. 28–30, 2000.

[13] Z. Zalevsky, D. Mendlovic, and R. G. Dorsch, "Gerchberg–Saxton algorithm applied in the fractional Fourier or the Fresnel domain," *Opt. Lett.*, vol. 21, pp. 842–844, 1996.

[14] H. E. Hwang, H. T. Chang, and W. N. Lie, "Multiple-image encryption and multiplexing using a modified Gerchberg-Saxton algorithm and phase modulation in Fresnel-transform domain," *Opt. Lett.*, vol. 34, pp. 3917–3919, 2009.

[15] Y. W. Huang, W. T. Chen, W. Y. Tsai, et al., "Aluminum plasmonic multicolor meta-hologram," *Nano Lett.*, vol. 15, pp. 3122–3127, 2015.

[16] W. Wan, J. Gao, and X. Yang, "Full-color plasmonic metasurface holograms," *ACS Nano*, vol. 10, pp. 10671–10680, 2016.

[17] X. Li, L. Chen, Y. Li, et al., "Multicolor 3D meta-holography by broadband plasmonic modulation," *Sci. Adv.*, vol. 2, p. e1601102, 2016.

[18] B. Wang, F. Dong, Q. T. Li, et al., "Visible-frequency dielectric metasurfaces for multiwavelength achromatic and highly dispersive holograms," *Nano Lett.*, vol. 16, pp. 5235–5240, 2016.

[19] Y. Montelongo, J. O. Tenorio-Pearl, W. I. Milne, and T. D. Wilkinson, "Polarization switchable diffraction based on subwavelength plasmonic nanoantennas," *Nano Lett.*, vol. 14, p. 294298, 2014.

[20] W. T. Chen, K. Y. Yang, C. M. Wang, et al., "High-efficiency broadband meta-hologram with polarization-controlled dual images," *Nano Lett.*, vol. 14, pp. 225–230, 2014.

[21] J. P. Balthasar Mueller, N. A. Rubin, R. C. Devlin, B. Groever, and F. Capasso, "Metasurface polarization optics: independent phase control of arbitrary orthogonal states of polarization," *Phys. Rev. Lett.*, vol. 118, p. 113901, 2017.

[22] M. Khorasaninejad, A. Ambrosio, P. Kanhaiya, and F. Capasso, "Broadband and chiral binary dielectric meta-holograms," *Sci. Adv.*, vol. 2, p. e1501258, 2016.

[23] F. Dong, H. Feng, L. Xu, et al., "Information encoding with optical dielectric metasurface via independent multichannels," *ACS Photonics*, vol. 6, pp. 230–237, 2019.
[24] L. Jin, Z. Dong, S. Mei, et al., "Noninterleaved metasurface for (2^6-1) spin- and wavelength-encoded holograms," *Nano Lett.*, vol. 18, pp. 8016–8024, 2018.
[25] W. Ye, F. Zeuner, X. Li, et al., "Spin and wavelength multiplexed nonlinear metasurface holography," *Nat. Commun.*, vol. 7, p. 11930, 2016.
[26] Q. Wei, L. Huang, X. Li, J. Liu, and Y. Wang, "Broadband multiplane holography based on plasmonic metasurface," *Adv. Opt. Mater.*, vol. 5, p. 1700434, 2017.
[27] L. Huang, H. Mühlenbernd, X. Li, et al., "Broadband hybrid holographic multiplexing with geometric metasurfaces," *Adv. Mater.*, vol. 27, pp. 6444–6449, 2015.
[28] F. Walter, G. Li, C. Meier, S. Zhang, and T. Zentgraf, "Ultrathin nonlinear metasurface for optical image encoding," *Nano Lett.*, vol. 17, pp. 3171–3175, 2017.
[29] X. Fang, H. Ren, and M. Gu, "Orbital angular momentum holography for high-security encryption," *Nat. Photon.*, vol. 14, pp. 102–108, 2020.
[30] M. Naor and A. Shamir, *Visual cryptography*, vol. 1–12, Berlin, Heidelberg, Advances in Cryptology – EUROCRYPT'94, 1995.
[31] S. J. Shyu, S. Y. Huang, Y. K. Lee, R. Z. Wang, and K. Chen, "Sharing multiple secrets in visual cryptography," *Pattern Recogn.*, vol. 40, pp. 3633–3651, 2007.
[32] A. Zhan, S. Colburn, R. Trivedi, T. K. Fryett, C. M. Dodson, and A. Majumdar, "Low-contrast dielectric metasurface optics," *ACS Photonics*, vol. 3, pp. 209–214, 2016.
[33] M. Khorasaninejad, W. Chen, R. Devlin, J. Oh, A. Y. Zhu, and F. Capasso, "Metalenses at visible wavelengths: diffraction-limited focusing and subwavelength resolution imaging," *Science*, vol. 352, pp. 1190–1194, 2016.
[34] A. Niv, G. Biener, V. Kleiner, and E. Hasman, "Propagation-invariant vectorial Bessel beams obtained by use of quantized Pancharatnam–Berry phase optical elements," *Opt. Lett.*, vol. 29, pp. 238–240, 2004.
[35] D. Lin, P. Fan, E. Hasman, and M. L. Brongersma, "Dielectric gradient metasurface optical elements," *Science*, vol. 345, pp. 298–302, 2014.
[36] H. S. Ee, J. H. Kang, M. L. Brongersma, and M. K. Seo, "Shape-dependent light scattering properties of subwavelength silicon nanoblocks," *Nano Lett.*, vol. 15, pp. 1759–1765, 2015.

Supplementary Material:: The online version of this article offers supplementary material (https://doi.org/10.1515/nanoph-2020-0298).